Plasma Sci. Technol. **19** (2017) 033001 (11pp) doi:10.1088/2058-6272/19/3/033001

Review

Understanding L–H transition in tokamak fusion plasmas*

Guosheng XU (徐国盛) and Xingquan WU (伍兴权)

Institute of Plasma Physics, Chinese Academy of Sciences, Hefei 230031, People's Republic of China

E-mail: xqwu@ipp.ac.cn

Received 6 May 2016
Accepted for publication 16 August 2016
Published 21 February 2017

Abstract

This paper reviews the current state of understanding of the L–H transition phenomenon in tokamak plasmas with a focus on two central issues: (a) the mechanism for turbulence quick suppression at the L–H transition; (b) the mechanism for subsequent generation of sheared flow. We briefly review recent advances in the understanding of the fast suppression of edge turbulence across the L–H transition. We uncover a comprehensive physical picture of the L–H transition by piecing together a number of recent experimental observations and insights obtained from 1D and 2D simulation models. Different roles played by diamagnetic mean flow, neoclassical-driven mean flow, turbulence-driven mean flow, and turbulence-driven zonal flows are discussed and clarified. It is found that the L–H transition occurs spontaneously mediated by a shift in the radial wavenumber spectrum of edge turbulence, which provides a critical evidence for the theory of turbulence quench by the flow shear. Remaining questions and some key directions for future investigations are proposed.

Keywords: L–H transition, $E\times B$ flow shear, turbulence suppression, zonal flows, Reynolds stress

(Some figures may appear in colour only in the online journal)

1. Introduction

As we know, when the heating power exceeds a threshold, the tokamak plasma can spontaneously transit from a low-confinement (L) state to a high-confinement (H) state due to the suppression of plasma turbulence and the formation of a transport barrier at the plasma edge, known as L–H transition. There is substantial evidence that the suppression of turbulence is due to the formation of a shear layer of $E \times B$ flows at the plasma edge [1, 2].

Since the L–H transition was first discovered in 1982 [3], it has been an old unsolved problem for three decades in the field of fusion plasma physics. Now that the H-mode is the projected baseline operational scenario for ITER [4], it is of great importance for understanding the physics basis for fusion energy. This topic of L–H transition is old, but still in progress, especially in the last five years, which is typically focused on two central questions. One is the mechanism for turbulence quick suppression at the L–H transition, and the other is the mechanism for the sheared-flow generation.

For the first question, many theories have been proposed. However, generally speaking, they can be divided into four categories.

(1) The mean flow bifurcation plus shear decorrelation, which is the most early proposed and also the most popular category of theories. The first theory is Stinger's spin up in 1969 [5]. Itoh [6, 7], Shaing [8], Biglari [9], and Hinton [10] all contributed to this category of theories. For this category, the shear decorrelation theory gives a rather weak dependence of the turbulence intensity with flow shear, such as the inverse square dependence [10, 11]. So, a significant increase of the mean flow shear in a very short time scale is required to

* This work was supported by National Magnetic Confinement Fusion Science Program of China under Contracts No. 2015GB101000, No. 2013GB106000, and No. 2013GB107000 and National Natural Science Foundation of China under Contracts No. 11575235 and No. 11422546.

suppress the turbulence to a low level. This sudden flow shear increase can only be achieved by a bifurcation of the momentum equilibrium at the plasma edge driven by a change in the neoclassical/turbulent momentum transport, momentum source/sink or momentum boundary condition. The ion orbit loss is one candidate mechanism belonging to this category [7, 8].

(2) The inverse cascade to zonal flows [12]. The plasma turbulence in a strongly magnetized plasma is thought to be quasi two dimensional. The inverse cascade to zonal flows is a fundamental property of the two dimensional turbulence. Based on this concept, Pat Diamond proposed the predator–prey model to explain the L–H transition [13, 14]. Following the logic of this theory, a prompt increase of the energy transfer rate from turbulence to zonal flows through the turbulent Reynolds stress is required.

(3) The radial wave number k_r spectral shift and tilt of turbulence eddy structures proposed recently by Gary Staebler based on the GYRO code simulations [15, 16]. The turbulence suppression is due to scattering turbulence energy to the high $k_\perp$ region where the energy is dissipated. This mechanism can explain the turbulence quench in the early gyro-fluid ITG turbulence simulations by Waltz [17].

(4) The phase transition across an instability boundary, for instance, stabilization of the resistive drift-ballooning mode at the L–H transition [18–20]. It is a candidate mode for the L-mode turbulence at the plasma edge.

For the second question: 'the mechanism for the sheared-flow generation', according to the radial force balance equation, which has been broadly studied in theories and experiments [18, 21–23], the total $E \times B$ flows are composed of the diamagnetic mean flow, the neoclassical-driven mean flow, the turbulence-driven mean flow and the turbulence-driven zonal flows which is the time-varying component. It is important to know that the mean flow can also have a turbulence-driven component. It is different from the zonal flows. In the H-mode pedestal, the diamagnetic mean flow dominates. However, in the L-mode plasma edge, these flow components may be comparable in magnitude.

In order to address these questions mentioned above for understanding the L–H transition in fusion plasmas, a series of experiments and model analyses have been extensively carried out on the EAST superconducting tokamak, then the main results and observations will be reviewed in this paper by the following sections. Section 2 briefly summarizes the contribution of different components to the sheared-flow generation. According to the radial force balance equation, (a) the diamagnetic mean flow dominates in the H-mode pedestal, however, neoclassical mean flow, turbulence-driven mean flow or turbulence-driven zonal flows may be comparable to the diamagnetic flow in the L mode, which bring in several feedback loops whereby E_r and its shear can change, allowing the plasma access to different confinement regimes. (b) Turbulence-driven mean flow is important, where the turbulence directly transports poloidal momentum out, which enhances the edge mean-flow shear in L mode. (c) Zonal flows are superimposed on the mean flow, which can trigger the transition when the mean-flow shear is still far below the transition threshold. If the zonal-flow amplitude is much smaller than the mean flow, the effects of zonal flows may be negligible, and the transition will be solely determined by the mean-flow shear. Section 3 presents an experimental evidence for the understanding of Waltz's turbulence quenching effects. It is found that the L–H transition occurs spontaneously mediated by a shift in the radial wavenumber spectrum of edge turbulence, which provides critical evidence for the theory of turbulence quench by the flow shear. Finally, section 4 contains conclusions and discussions of open questions.

2. Mechanism for the sheared-flow generation

Considering that the plasma is a self-consistent system of force balance, $E \times B$ flow V_E is determined by the radial electric field E_r, which in turn could be deduced from the radial force balance for any plasma species. Since the main ions dominate the plasma momentum due to their large mass relative to electrons, it is of interest to $E \times B$ flow on the ion species shown in equation (1). The sign convention here is that the positive value designates in the ion diamagnetic drift direction and the negative value designates in the electron diamagnetic drift direction

$$V_E = \frac{\nabla p_i}{Z_i e B n_i} + V_{i\perp} + v_{i\perp}, \tag{1}$$

where Z_i is the charge state of the ions, e is the electronic charge, n_i is the ion number density, and p_i is the ion pressure. All quantities in equation (1) have been averaged over magnetic-flux surfaces, the terms on the right-hand side represent the following processes. The first one $\frac{\nabla p_i}{Z_i e B n_i}$ is the diamagnetic mean flow which is determined by the power balance involving the cross-field heat, particle transport. The second one $V_{i\perp}$ is the perpendicular mean flow, which could be decomposed into the poloidal and toroidal two components in a torus shown in equation (2) involving the neoclassical and turbulent poloidal and toroidal momentum transport. The contribution of co-current toroidal rotation to $E \times B$ flow is in the ion diamagnetic drift direction

$$V_{i\perp} = V_{i\theta}\frac{B_\phi}{B} - V_{i\phi}\frac{B_\theta}{B}. \tag{2}$$

The third one $v_{i\perp}$ means turbulence-driven zonal flows [12, 24], it is superimposed on the mean flow to give $E \times B$ flow a significant time-varying and spatial varying component. Recently these effects have been directly observed by the high spatial resolution Doppler backscattering measurements in JET [25]. Therefore, zonal flows could also play a very important role in the sheared-flow generation, and eventually help to stabilize the turbulence for L–H transition trigger as shown in the schematic diagram of figure 1. The zonal flows are fluctuating flows, which is possible to make the flow shear exceed the threshold instantaneously, thus to trigger the transition when the mean-flow shear is still far

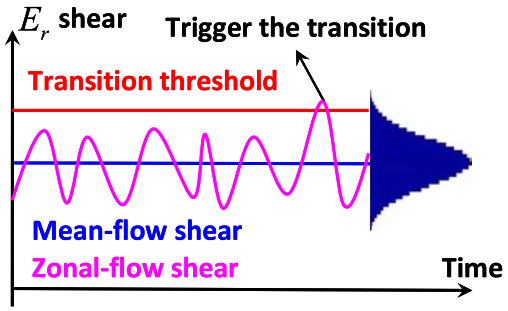

Figure 1. Zonal flows are superimposed on the mean flow, which can trigger the transition when the mean-flow shear is still far below the transition threshold.

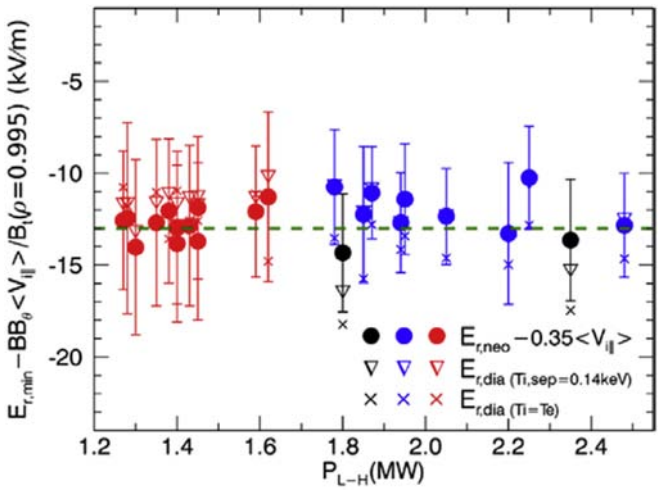

Figure 2. The minimum of E_r is independent of the heating power and even wall materials. Reproduced with permission from [27], copyright 2016 IOP Publishing.

below the transition threshold. Therefore, the zonal flows in principle can reduce the transition threshold.

However, if the zonal-flow amplitude is much smaller than the mean flow, the effect of zonal flows may be negligible, and the transition will be solely determined by the mean-flow shear. In the ASDEX-Upgrade, it is found that the E_r minimum at the plasma edge prior to the L–H transition does not change with the pedestal density [26]. The more recent investigations indicate that the minimum of E_r is also independent of the heating power and even wall materials [27], shown in figure 2, suggesting that in ASDEX-Upgrade the mean flow shear dominates the transition threshold. (There are some deviations, which may be due to the zonal flows, but they are relatively small.)

2.1. The role played by poloidal mean flow in sheared-flow

Particularly, the statement of this paper is focusing on the plasma edge physics of the L–H transition, which implies that the diamagnetic and poloidal mean flow dominate $E \times B$ flow [2]. Due to the very small projection in a tokamak and the approximate toroidal symmetry, the toroidal neoclassical stress is relatively weak [28, 29], which means near the edge the contribution from the toroidal mean flow is generally thought to be small. However, it is capable of shifting the $E \times B$ flow profile and affecting the transition power. Therefore, in the edge region the approximation of the $E \times B$ mean flow could be given by equation (3), where the perpendicular mean flow is dominated by its poloidal components

$$V_E \approx \frac{\nabla p_i}{Z_i e B n_i} + V_{i\theta}. \tag{3}$$

According to equation (3), to explore the dynamic evolution of $E \times B$ mean flow requires access to the cross-field heat, particle transport and cross-field poloidal momentum transport, which involve different feedback loops between turbulence and $E \times B$ sheared flow [30]. For the poloidal mean flow $V_{i\theta}$, it can be driven by the turbulent transport through the turbulent Reynolds stress [31], which is the turbulence-driven momentum flux. It can also be strongly influenced by the neoclassical transport, where the poloidal neoclassical stress is strong in a tokamak due to the very strong magnetic pumping [28, 32, 33] and the ion-orbit loss at the plasma edge [7, 8]. These processes are coupled together to determine the profile of poloidal mean flow, which have been estimated in a radial dynamic model via equation (4) [30, 34]

$$(1 + 2q^2)\partial_t V_{i\theta} = -\partial_r \langle \tilde{v}_{i\theta} \tilde{v}_{ir} \rangle - \mu_\theta^{neo}(V_{i\theta} - V_{i\theta}^{neo}) \times -\Gamma_{ion-orbit\ loss} + \Gamma^{bV}. \tag{4}$$

Another important factor that makes the plasma edge special is the boundary conditions. In the core, the poloidal flow is usually clamped to the neoclassical value due to the very strong magnetic pumping. However, at the plasma edge, the E_r in the SOL is usually positive due to the sheath boundary condition and the radial decay of the electron temperature [34–36], the related approximate expression could be given by $E_r \approx -2.8\partial_r T_e/e$. Then from the point of view of poloidal flow, $E \times B$ flow is fixed at the edge in the dynamic model, which leads to a constrained boundary condition for equation (4) by the radial force balance equation, shown as equation (5)

$$V_{i\theta}\,|_{r=a} = \left(-\frac{\nabla p_i}{Z_i e B n_i} + V_E\right)|_{r=a}, \tag{5}$$

where influence from the toroidal mean flow is also neglected, and the suitable edge values of temperature and density are required to match the heat flux into the crape-off layer (SOL) [37, 38].

As the comprehensive result of the radial force balance equation is near the edge, figure 3 visualizes the profile of the $E \times B$ flow and its two important components in L-mode from equation (3), where the poloidal flow near the separatrix significantly deviates from the neoclassical value $V_{i\theta}^{neo}$. A viscous boundary layer is formed inside the separatrix to

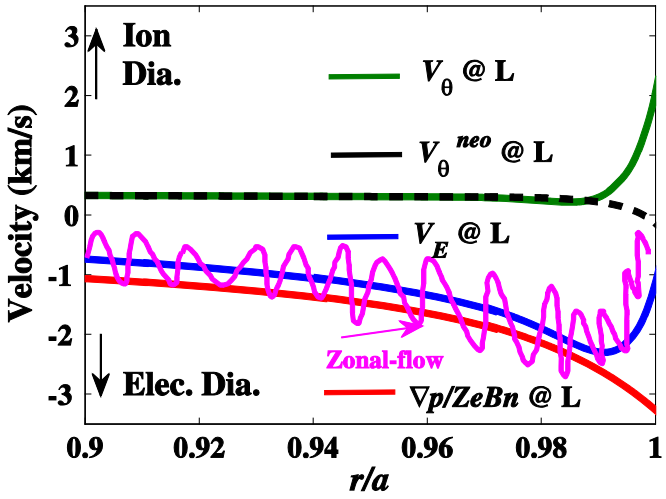

Figure 3. The profiles of the $E \times B$ flow, the poloidal flow and the diamagnetic flow from the radial force balance equation at L-mode estimated by the radial dynamic model [30], where zonal flow is schematically superimposed on the mean flow. Reproduced with permission from [30], copyright 2015 IAEA.

transition from the SOL poloidal flow to the neoclassical solution in the core. It is obvious that there is a sharp shear layer of poloidal flow near the edge since there is a big velocity gap between the neoclassical flow and the diamagnetic flow. The negative radial electric field well E_r-well is formed near the inside of the edge, where the pressure gradient determining the depth of the E_r-well and poloidal flow give the positive contribution to make the E_r have a fixed value at the edge. Also schematically the zonal flow is superimposed on the mean flow to give E_r a fine-scale structure [25]. In the L-mode, the E_r-well is relatively low and flat due to the shallow pressure gradient. However, a sharp flow shear component by poloidal flow near the edge implies that before the diamagnetic flow becomes dominating, the modulation of poloidal flow by the momentum transport will highly affect the total $E \times B$ flow shear.

Furthermore, the modeling of dynamic evolution for the edge poloidal flow is also in close compliance with the relevant experiments, where direct evidence has been reported that the edge poloidal flow and $E \times B$ flow change across the L–H transition were measured 20 years ago in DIII-D [22, 39]. Just as shown in figure 4 of the recent results from the 1D radial dynamic model [30], which successfully reproduced the profiles change across the L–H transition, the edge E_r becomes more negative in the H-mode mainly due to the significant increase of the diamagnetic mean flow. However, its boundary value on the separatrix is still clamped to a positive value due to the sheath boundary condition in the SOL. The poloidal mean flow at the plasma edge increases in the ion-diamagnetic direction across the L–H transition mainly due to the boundary condition change, namely, significant increase of the pressure gradient and the diamagnetic mean flow on the separatrix.

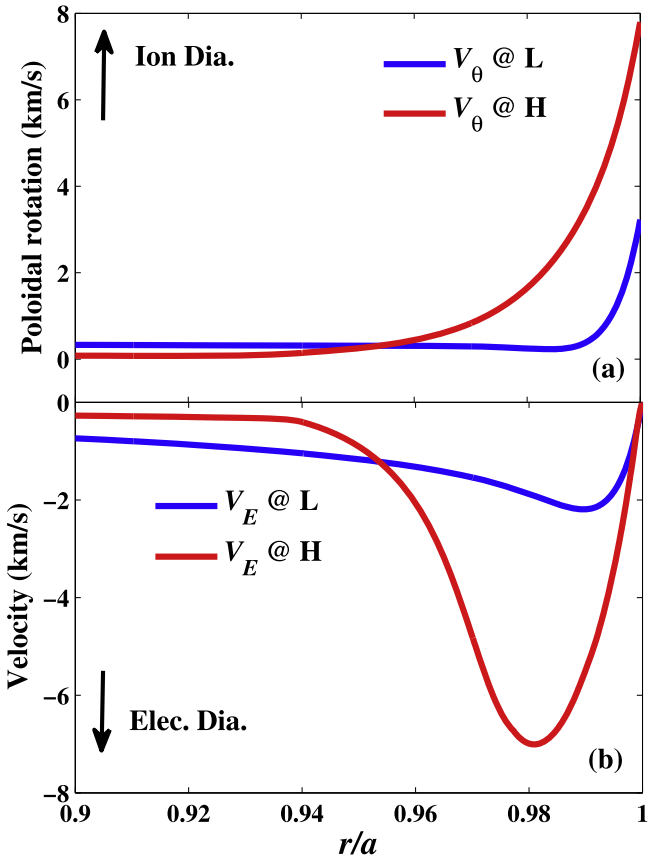

Figure 4. The profiles of the poloidal flow (a) and $E \times B$ flow (b) at L-mode and H-mode in the edge region by the radial dynamic model. Reproduced with permission from [30], copyright 2015 IAEA.

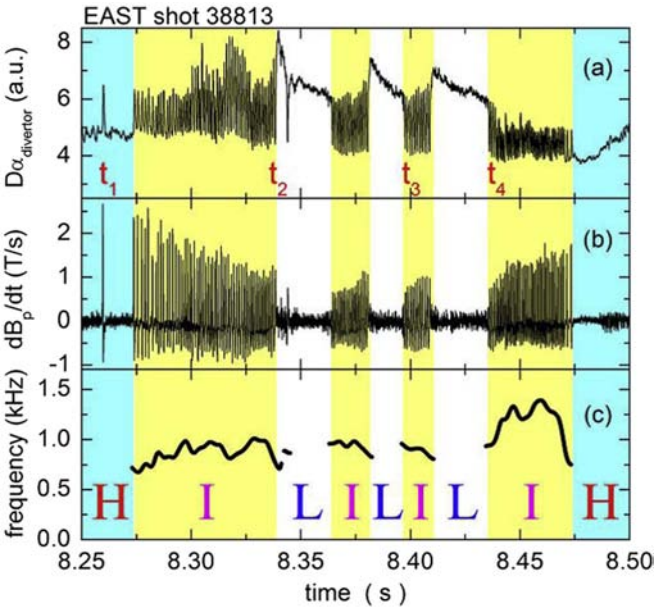

Figure 5. The time history of (a) divertor Dα emission, (b) magnetic signal measured by the No.7 Mirnov probe, and (c) oscillation frequency based on Fourier analysis. Reproduced with permission from [36], copyright 2014 IAEA.

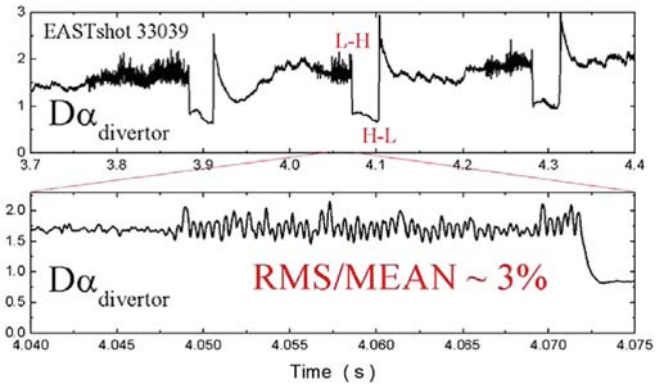

Figure 6. The time history of (a) divertor Dα emission and (b) its zoom-in plot for small dithering. Reproduced with permission from [36], copyright 2014 IAEA.

2.2. The role played by the turbulence-driven mean flow in the L–H transition

Since the poloidal flow provides a sharp flow shear component near the edge, the poloidal momentum transport with turbulence could be very important during L–H transition. Actually, near the transition power threshold, there is an oscillatory intermediate phase, so-called I-phase, as shown in figure 5, which can occur at L–H transition, H–L back transition or during the L mode, namely, the normal dithering. It should be clarified that the flow oscillations that appear during the I-phase are not zonal flows; they are oscillating mean flows [36], which is a significant phenomenon to analyze the momentum transport of turbulence-driven mean flow.

In contrast with the normal dithering, a small dithering was also observed prior to the L–H transition near the power threshold firstly in EAST [36, 40] shown in figure 6, and observed in other tokamaks, such as the ASDEX-Upgrade [41]. This small dithering is different from the normal dithering in the I-phase. For instance, it has very weak magnetic perturbations, typically less than 0.1 Gauss. However, the normal dithering in the I-phase has very strong $n = 0$, $m = 1$ magnetic perturbations [36, 42], typically of 1 Gauss, more than ten times larger. In addition, it is observed that the turbulence suppression and turbulent Reynolds stress modulation are associated with the small dithers, which is consistent with the characteristics of zonal flows [40].

Now from the view point of mean flow, the natural question is: what is the role played by the turbulence-driven mean flow in the L–H transition? Especially, it is necessary to know whether the turbulence-driven mean flow enhances or reduces the mean flow shear in the L-mode plasma edge? In JET, with the reciprocating probe measurements, it was found that turbulence transports positive poloidal momentum out through the turbulent Reynolds stress [43], as shown in figure 7. Since the poloidal mean flow on the separatrix is determined by the boundary condition, the outward turbulent momentum flux will reduce the positive poloidal mean flow, thus enhancing the mean flow shear at the plasma edge in the L mode. Therefore, the turbulence-driven mean flow in principle can reduce the L–H transition threshold and trigger the transition.

As shown in figure 8, in EAST, sometimes, it is clearly observed that the turbulence level, turbulent Reynolds stress, mean flow and mean flow shear increase prior to the L–H transition [36, 44]. A similar phenomenon has also been observed recently in DIII-D [45, 46] and Alcator C-Mod [47] with different diagnostics. However, just like near the L–H transition, the minimum of E_r is independent of the heating power and even wall materials shown in figure 2, so it is highly suggested that the transition threshold is determined by the total $E \times B$ flow shear not the turbulence-driven mean flow shear. How strongly can the turbulence-driven mean flow influence the transition threshold, which is thought to be a problem of the relative contribution to the total flow shear.

Meanwhile, how does the $E \times B$ flow and flow shear change during the L–H transition? Dedicated experiments have been conducted on EAST with a 3 by 4 probe array [36]. As shown in figure 9, the probe measurements indicate that the mean $E \times B$ flow near the separatrix changes towards the ion-diamagnetic direction, and the flow shear increases at the same time of the turbulence suppression. Since the turbulence-driven mean flow will disappear when the turbulence is suppressed, and the pressure gradient increases near the separatrix, this may lead to the recovery of the turbulence level and the formation of limit-cycle oscillations (LCOs). The diamagnetic mean flow keeps building up, and finally the plasma locks in the H mode. If the diamagnetic mean flow cannot immediately take over, for instance, because the pressure gradient increase is very slow in the marginal power case, a LCO will appear.

For the LCOs, figure 10 shows the L–I–H transition measured by the gas puff imaging diagnostics in EAST [48, 49]. Recently, the L–I–H transition and back transition have been successfully reproduced by the HESEL code, which is a four-field 2D drift-MHD code [50, 51], as shown in figure 11. The simulation domain is a rectangle area on the low-field side near the outer midplane. The simulation recovers the transition power threshold as well as the decrease in power threshold switching from a single to double null configuration observed in the EAST experiments. The key to achieving the simulations of L–H transition and I-phase is the introduction of the generalized vorticity $\omega = \nabla^2(\phi + p_i)$, which could be derived from the leading order polarization current and numerically applied by other models [52–54]. It has a term proportional to the time derivative of the ion pressure gradient, which is essential for setting up and sustaining the 'mean flow', which locks plasma in the H mode.

3. Understanding of turbulence quenching effects

3.1. Dynamic model of turbulence radial wavenumber spectrum shift

Comparing with the observation of plasma parameters change during L–H transition, it is more difficult to directly evidence a turbulence suppression theory with finite plasma

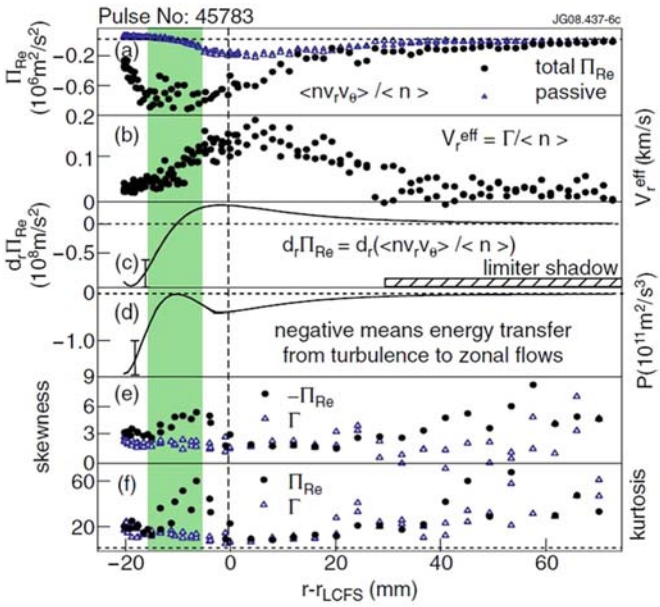

Figure 7. The radial profiles of (a) total and passive momentum fluxes; (b) effective radial velocity; (c) radial gradient of momentum flux; (d) energy transfer rate between turbulence and zonal flows; (e) skewness and (f) kurtosis of Reynolds stress and particle flux. Reproduced with permission from [43], copyright 2009 IAEA.

diagnostics. Therefore, instead of addressing the first general question of how does the flow shear suppress the turbulence during the L–H transition, here a special question is specified: what is the physics behind the 'Waltz's quench rule', namely, turbulence quenches when the $E \times B$ shearing rate exceeds the linear growth rate of the most unstable mode [17]. As a paradigm, the reduction of the intensity of the turbulence I was found to be well fit over a range of plasma parameters by equation (6)

$$I = I_0 \,\mathrm{Max}\left[1 - \frac{\alpha_{\mathrm{E}}\,|\gamma_{E\times B}|}{\gamma_{\max}}, 0\right], \tag{6}$$

where I_0 is the turbulence intensity without the $E \times B$ velocity shear $\gamma_{E\times B}$, $\gamma_{\max}$ is the maximum linear growth rate without $E \times B$ flow shear, and α_{E} is a proportional factor.

On the other hand, the shear decorrelation theory of Shaing [8] or Biglari [9] gives a rather weak dependence of the turbulence intensity on flow shear. An example [11] of the formula for the reduction of the turbulence intensity due to the decorrelation effect is shown as equation (7)

$$I = I_0/[1 + (\alpha_{\mathrm{cor}}\gamma_{E\times B}\tau_{\mathrm{c0}})^2], \tag{7}$$

where τ_{c0} is the decorrelation time of the turbulence without mean field $E \times B$ flow shear, and α_{cor} is a proportional constant.

If one is to define a reduced function of $E \times B$ flow shear $f(\gamma_{E\times B})$ for each of equations (6) and (7), it is possible to illustrate the comparison between turbulence quench and decorrelation, where the normalized turbulence intensity varies with a reduced function of $E \times B$ flow shear shown in figure 12. The formula of equation (7) could be capable of providing a bifurcation to an improved particle and energy confinement similar to the H-mode regime [10]. In the past, the decorrelation theory was tested with non-linear gyro-fluid simulations of ion temperature gradient (ITG) modes with adiabatic electrons in torodial geometry [55, 56]. Surprisingly, it was found that the stabilizing effect of $E \times B$ flow shear was an order of magnitude stronger than the decorrelation formulas would predict.

Furthermore, the turbulence suppression in experiments usually occurs very fast, typically of 100 μs [57]. Thus a significant increase of the mean flow shear in a very short time scale is required for the decorrelation paradigm to suppress the turbulence at the transition. However, the mean flow change prior to the transition is usually small. So, there is a causality problem. The turbulence intensity may have a much stronger nonlinear dependence with the flow shear.

In order to understand the turbulence quenching effects, a more recent turbulence suppression theory was proposed by Gary Staebler based on the GYRO code simulations [15, 16]. In this theory, the turbulence suppression is induced by a radial wavenumber spectral shift k_{r} and a tilt of 2D eddy structures due to the breaking down of the ballooning symmetry in a torus by the flow shear. The spectral shift scatters turbulence energy to the high $k_\perp$ region where the energy is dissipated. Based on this suppression mechanism, a dynamic model of turbulence radial wavenumber spectrum shift has been developed, which has the advantage of demonstrating that the fast transition can occur spontaneously, mediated by a shift in the radial wavenumber spectrum of turbulence without the assistance of zonal flows [58]. The model consists of two coupled dynamic equations

$$\frac{\partial \Phi}{\partial t} = \gamma_{k_y}\Phi + \gamma_{E\times B}k_y\frac{\partial \Phi}{\partial k_x} - (c_y k_y^2 + c_x k_x^2)\Phi^2 + D_\Phi\frac{\partial^2 \Phi}{\partial k_x^2}, \tag{8}$$

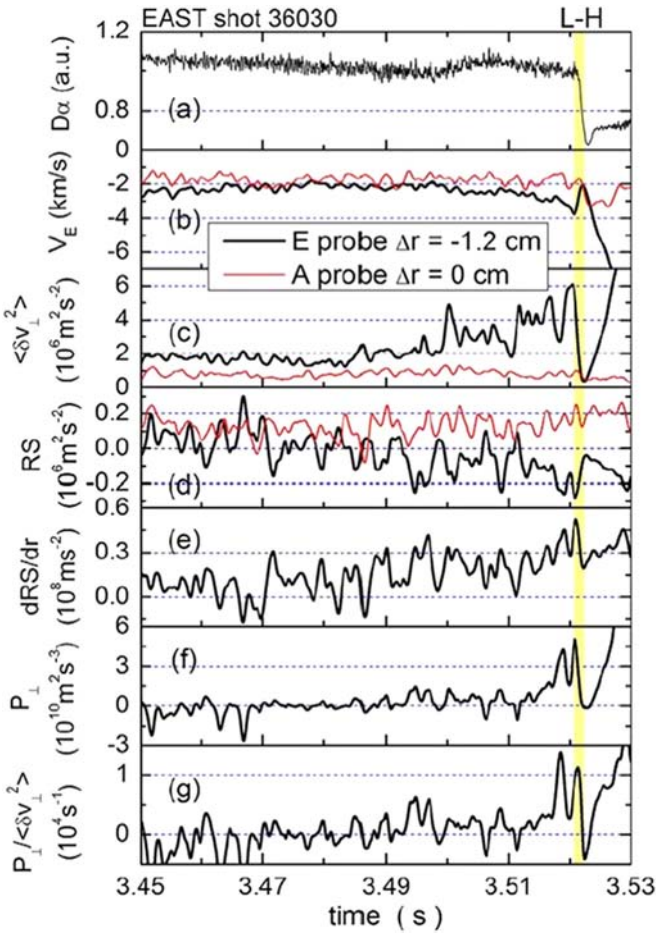

Figure 8. The time history of (a) divertor Dα emission, (b) $E \times B$ velocities, black and red curves standing for that measured at ports E and A, respectively, (c) mean-square fluctuation levels of the perpendicular $E \times B$ flows, (d) turbulent Reynolds stress, (e) the radial gradient of turbulent Reynolds stress, (f) shear flow production, and (g) normalized shear flow production. Reproduced with permission from [36], copyright 2014 IAEA.

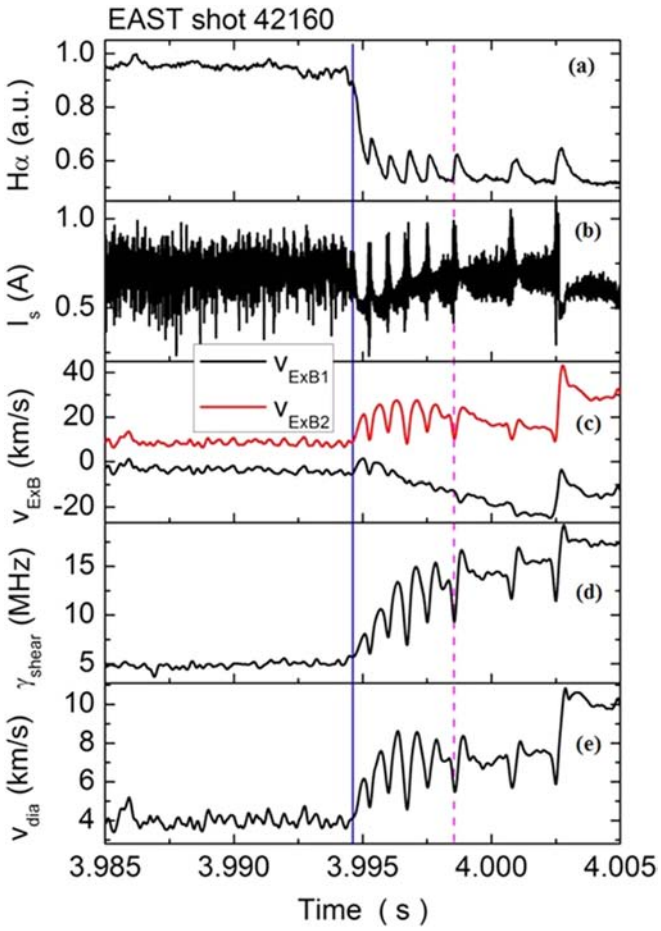

Figure 9. The time history of (a) divertor Hα emission, (b) ion saturation current from the innermost tip, (c) $E \times B$ flow velocity at $\Delta r \sim -5$ mm (black) and at $\Delta r \sim 0$ mm (red), (d) $E \times B$ flow shear, and (e) electron diamagnetic drift velocity.

$$\frac{\partial\,|\nabla p|}{\partial t} = Q_{\rm eff} - (\chi_{\rm eff} + \chi_{\rm eff}^{\rm neo})|\nabla p|, \qquad (9)$$

where the details of the model are discussed in [57], so it is suitable to briefly outline the essential framework here.

Equation (8) is a time-dependent one-dimensional (in k_x space) equation describing the nonlinear evolution of the amplitude of the electric potential fluctuations Φ [15], which corresponds to turbulence intensity $I \propto \Phi^2$. $k_x = k_r \rho_s$ is the radial wave number, $k_y = k_\theta \rho_s$ is the poloidal wave number, and ρ_s is the ion gyroradius. On the right-hand side of equation (8), the γ_{k_y} in the first term indicates the turbulence increases by the linear growth rate of the most unstable mode at a certain k_y. For the tokamak plasma edge region, γ_{k_y} could be evaluated via the ballooning-type instabilities driven by pressure gradient ∇p. The second term describes the shift in the radial wave number spectrum induced by the shear in fluctuation phase velocity in the lab frame, the so-called 'Doppler shift' [17]. If the shear is dominated by $E \times B$ shear $\gamma_{E\times B}$, it can be tied to the ion pressure gradient according to the radial force balance equation. The third term is a quadratic nonlinear term, which represents the effect of nonlinear mode coupling and viscous dissipation, leading to turbulence damping. Since the actual nonlinear mode coupling term in the gyrokinetic equation is a convolution over the (k_x, k_y) space [15, 59], the fourth term of spectral diffusivity has been used to recover the mode coupling between adjacent k_x.

Equation (9) describes the cross-field thermal transport at the plasma edge. $Q_{\rm eff}$ is the heat flux from the plasma core, which is proportional to input heating power. $\chi_{\rm eff}^{\rm neo}$ is the neoclassical thermal conductivity. $\chi_{\rm eff} \propto \int_{-k_{x\,\max}}^{k_{x\,\max}} k_y \Phi^2 {\rm d}k_x$ is the turbulence-driven thermal conductivity. $\chi_{\rm eff} >> \chi_{\rm eff}^{\rm neo}$ needs to be satisfied in L-mode plasmas. Finally, the pressure gradient contributes to the turbulence driving and $E \times B$ shear, and the turbulence intensity dominates the thermal transport; these processes make equations (8) and (9) couple to each other.

The main modeling results are shown in figures 13 and 14. The system reaches a stationary state first, which is an L-mode state far from the transition threshold condition. When the input heating power is doubled shown in

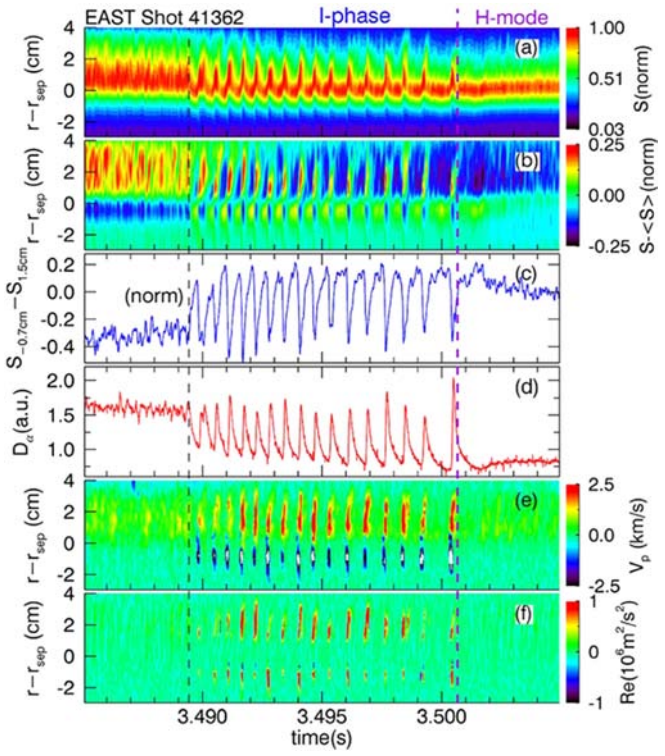

Figure 10. EAST shot No.41362 with input power slowly ramped up revealing the essential features of the L–I–H transition. The frames show measurements from the confined region ($r < 0$) and the region with open field lines—the SOL ($r > 0$). (a) The emission intensity of the HeI line, S, (b) the fluctuation level of S, (c) the difference in the relative GPI emission intensity between radial positions $r = -7$ mm and $r = 15$ mm, (d) the Dα emission from the outer divertor region, (e) poloidal flow velocity from GPI, and (f) turbulence-driven Reynolds stress with fluctuations in the perpendicular velocities derived from GPI [48, 50]. Reproduced with permission from [50], copyright 2015 Elsevier.

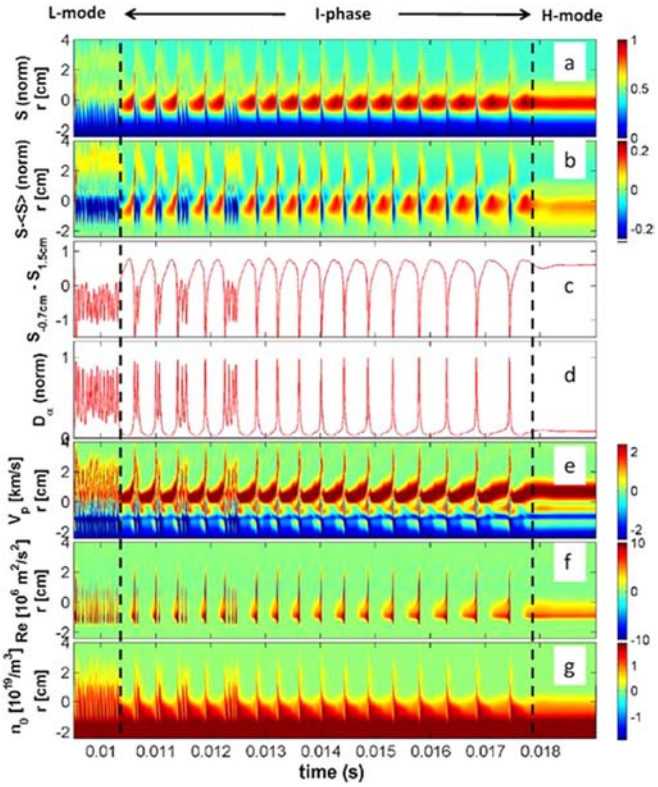

Figure 11. HESEL simulation for plasma parameters of EAST shot No.41362 similar to figure 1. (a) to (c) derived from a synthetic GPI signal, (d) integrated parallel particle loss term as a proxy to divertor Dα, (e) and (f) derived from $E \times B$ velocities, and (g) displays the electron density profile not accessible from GPI. Reproduced with permission from [50], copyright 2015 Elsevier.

figure 13(e), the edge pressure gradient and turbulence amplitude gradually climb up to a higher level and then nearly saturate. However, the k_x-spectrum continuously evolves as approaching the transition, as indicated by the evolution of the spectral average shift $\langle k_x \rangle$ which is defined by $\langle k_x \rangle = \int_{-k_{x\,\max}}^{k_{x\,\max}} k_x \Phi^2 \mathrm{d}k_x \Big/ \int_{-k_{x\,\max}}^{k_{x\,\max}} \Phi^2 \mathrm{d}k_x$ .The physics direction of negative k_x is radially outward, which is the same as that in the experiments. In particular, the change in $\langle k_x \rangle$ accelerates near the transition point, suggesting an accelerated spectral shift, which eventually triggers the L–H transition. At the transition, the turbulence amplitude is quenched within a few hundreds of microseconds due to a fast spectral shift as shown in figure 14(b). The fast spectral shift leads to a quick suppression of the turbulence by the nonlinear mode coupling and dissipation in the third term of equation (8). The Reynolds stress is defined by the quasilinear formula, $\mathrm{Re} = \int_{-k_{x\,\max}}^{k_{x\,\max}} k_y \Phi^2 \mathrm{d}k_x$. It does not show a pre-transition overshot, instead, it decreases as approaching the transition due to a reduced integral of the spectral power by the spectral shift, and then quickly decreases at the transition when the turbulence amplitude is suppressed.

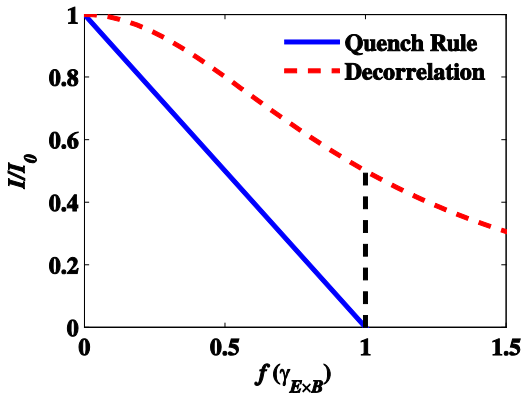

Figure 12. Schematic diagram of normalized turbulence intensity versus a reduced function of $E \times B$ flow shear.

3.2. Direct evidence for the turbulence radial wavenumber spectral shift

The turbulence suppression mechanism and the dynamic model as shown above could explain the turbulence quench in the early gyro-fluid ITG turbulence simulations. Even a model has been developed based on this suppression theory, which has successfully reproduced the fast L–H transition and the LCOs in the I-phase [60, 61]. But another important

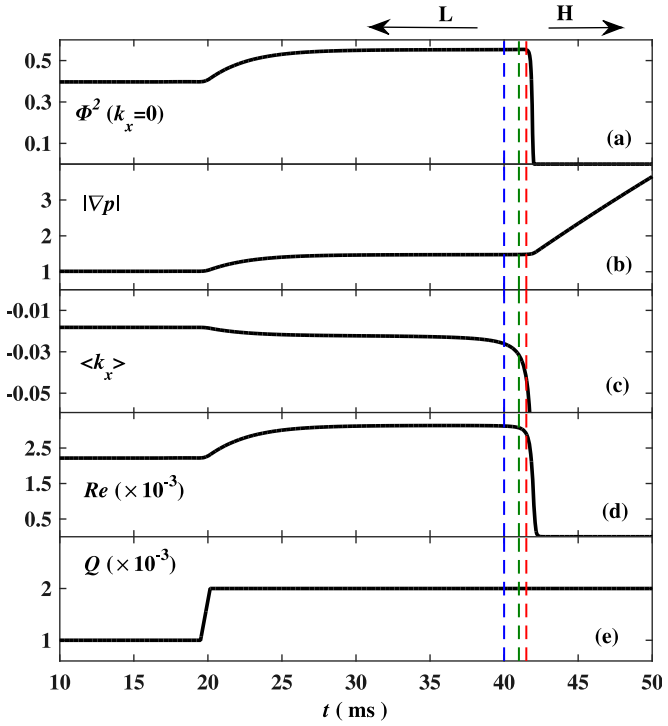

Figure 13. Time evolution of (a) turbulence amplitude at $k_x = 0$, (b) edge pressure gradient, (c) spectral-averaged $\langle k_x \rangle$, (d) turbulent Reynolds stress, and (e) heat flux from the plasma core.

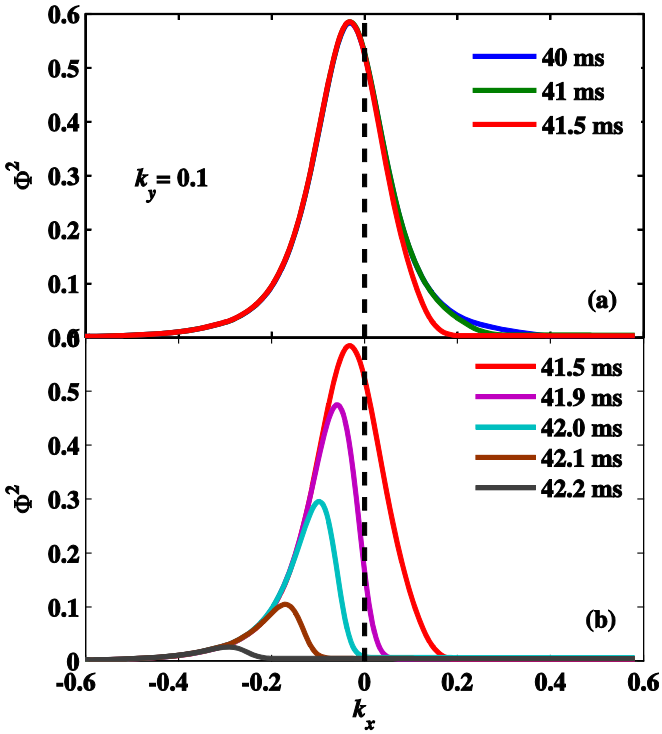

Figure 14. The k_x spectra at several time points with corresponding colors as indicated in the insets, (a) in the L mode near the power threshold, and (b) within about 1 ms across the L–H transition.

experimental fact on EAST should be mentioned to further validate the turbulence quenching effects.

More recently, the direct observation of an L–H transition mediated by the turbulence k_r spectral shift and eddy structure tilting has been achieved, for the first time, in the EAST superconducting tokamak [58]. As shown in figure 15, the turbulence k_r spectral shift appears tens of milliseconds prior to the L–H transition indicated by a sharp drop in the divertor Dα emission level, correlated with the time evolution of the local $E \times B$ flow shear at the plasma edge. The amplitude of turbulent Reynolds stress does not show significant change prior to the transition, instead, it decreases at the transition when the turbulence level is suppressed. Here, negative k_r points outwards radially. The change in the spectral shape is mainly manifested by a depletion of the spectral power on the positive k_r side, consistent with the modeling results as shown in figure 14(a).

Across the transition, the spectral shift is significantly accelerated, as indicated by the inclined spectral transition front marked by the dashed line in figure 16(a), which is the zoom-in plot of figure 15(a) near the transition point. The k_r spectrum moves completely to the negative k_r side; meanwhile, the turbulence level is significantly reduced within a few hundreds of μs, just like those predicted by the model in figure 14(b). Figure 16(b) shows the turbulence power spectra in (k_r, k_θ) space at three time points indicating that the tilting angle of the turbulence structures increases as approaching the transition point in addition to the spectral shift towards negative k_r. The spectra concentrate mostly in the negative k_θ space, since the turbulence propagates poloidally in the electron diamagnetic direction in the lab frame.

4. Conclusions and discussions

According to the experiments and model analysis carried out on the EAST superconducting tokamak for understanding the L–H transition in fusion plasmas, the main results and observations have been summarized in this paper for the turbulence quick suppression mechanism and the sheared-flow generation at the L–H transition.

For the turbulence quick suppression, it is challenging for the shear decorrelation paradigm. However, the direct observation of a turbulence radial wavenumber spectral shift and turbulence structure tilting prior to and across the L–H transition at the plasma edge in EAST may shed light on the recent experimental observations concerning the L–H transition process. According to this new turbulence suppression mechanism, i.e., scattering turbulence energy to a higher $k_\perp$ region instead of inverse cascading to zonal flows, a bifurcation driven solely by the mean flow shear is possible. Furthermore, the bifurcation is not necessarily triggered or preceded by a sudden increase in the mean flow shear. The increase of mean flow shear typically occurs right after the transition as a consequence of the turbulence suppression.

It should be noted that the shear in fluctuation phase velocity in the lab frame v_{ph} is composed of $E \times B$ drift velocity V_E and phase velocity in the plasma frame v_{php}, which

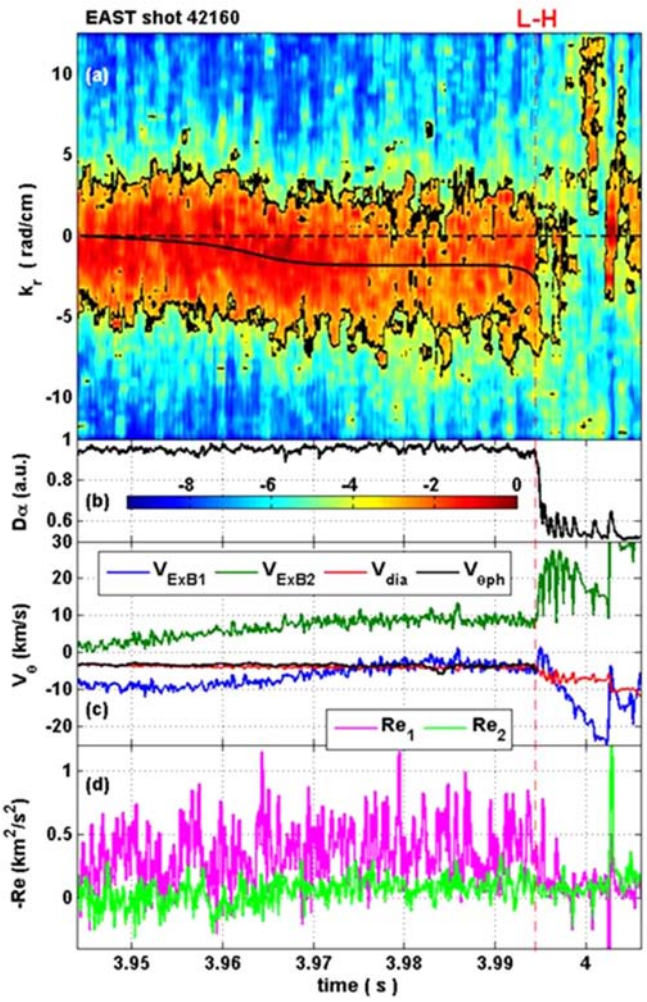

Figure 15. Direct evidence for the turbulence radial wavenumber spectral shift prior to and mediating the L–H transition obtained at plasma edge in EAST using a probe array. Time evolution of (a) radial wavenumber spectrum displayed in log scale, spectral averaged radial wavenumber $\langle k_r \rangle$ as indicated by the black curve, (b) Divertor Dα emission, (c) $E \times B$ velocity at two radial locations, diamagnetic drift velocity and poloidal phase velocity of fluctuations, (d) turbulent Reynolds stress at ~5 mm inside the separatrix for Re_1 and approximately on the separatrix for Re_2. Reproduced with permission from [58], copyright 2016 American Physical Society.

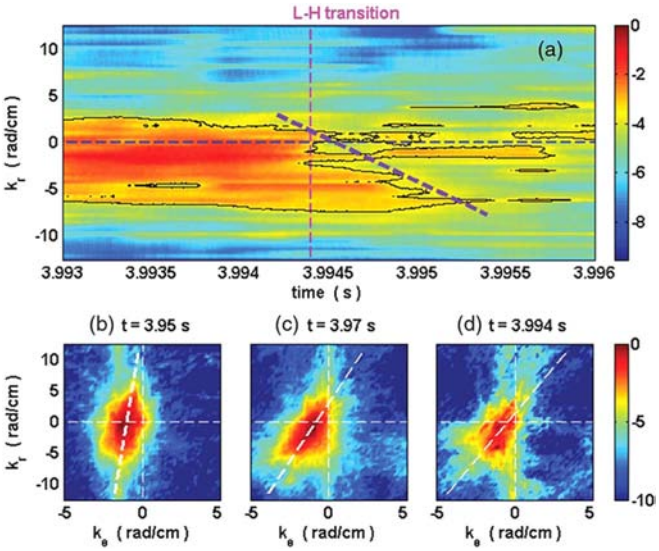

Figure 16. (a) Time history of k_r spectrum near the L–H transition. (b)–(d) Power spectra in (k_r, k_θ) space at three time points: $t = 3.95$ s (40 ms before the transition), $t = 3.97$ s (20 ms before the transition), $t = 3.994$ s (just prior to the transition). Reproduced with permission from [58], copyright 2016 American Physical Society.

means some changes in v_{php} due to some modifications in the turbulence modes can also lead to v_{ph} change even though there is no change in V_E. Therefore, besides the $E \times B$ flow shear, other effects contributing to the shear in v_{ph} also should be studied further theoretically and experimentally.

For the sheared-flow generation, especially for the $E \times B$ flow shear, the radial force balance equation is a direct tool to examine the change of radial electric field, which indicates $E \times B$ flow can be generated spontaneously through several mechanisms, such as a steepening of the ion pressure gradient, ion orbit loss, plasma rotation, or turbulence-driven momentum transport via turbulent Reynolds stress. Particularly at the tokamak edge, it is necessary to investigate the boundary condition of SOL and the direction of turbulence-driven momentum flux carefully, since the poloidal flow near the separatrix could significantly deviate from the neoclassical value, which provides a sharp flow shear component for $E \times B$ flow shear near the edge.

Meanwhile it is emphasized that turbulence-driven zonal flow superimposed on the mean flow gives $E \times B$ flow a significant time-varying and spatial varying component. Therefore, zonal flows could also play a very important role in the sheared-flow generation for the LCOs during slow L–H transition near the transition power threshold.

Another key factor in L–H transition modeling that should be marked out is the generalized vorticity $\omega = \nabla^2(\phi + p_i)$, which could be derived from the leading order polarization current and related to MHD type instabilities. Thereby it is implied that the L–H transition could be associated with the stabilization of the MHD type mode near the separatrix since k is very small and the parallel electron motion is strongly impeded, and as a consequence a new MHD type of instabilities may arise near the separatrix.

Finally, the recent work on EAST still cannot fully uncover the mystery of L–H transition, but these findings mentioned above represent a substantial and novel advance in this important area of magnetic fusion research, which may open a new path of inquiry in future work.

References

[1] Moyer R A *et al* 1995 *Phys. Plasmas* **2** 2397
[2] Burrell K H 1997 *Phys. Plasmas* **4** 1499
[3] Wagner F *et al* 1982 *Phys. Rev. Lett.* **49** 1408
[4] Shimada M *et al* 2007 *Nucl. Fusion* **47** S1
[5] Stringer T E 1969 *Phys. Rev. Lett.* **22** 770
[6] Itoh K 1994 *Plasma Phys. Control. Fusion* **36** A307
[7] Itoh S I and Itoh K 1988 *Phys. Rev. Lett.* **60** 2276
[8] Shaing K C and Crume E C 1989 *Phys. Rev. Lett.* **63** 2369

[9] Biglari H, Diamond P H and Terry P W 1990 *Phys. Fluids* B **2** 1
[10] Hinton F L and Staebler G M 1993 *Phys. Fluids* B **5** 1281
[11] Zhang Y Z and Mahajan S M 1992 *Phys. Fluids* B **4** 1385
[12] Diamond P H *et al* 2005 *Plasma Phys. Control. Fusion* **47** R35
[13] Kim E J and Diamond P H 2003 *Phys. Rev. Lett.* **90** 185006
[14] Diamond P H *et al* 1994 *Phys. Rev. Lett.* **72** 2565
[15] Staebler G M *et al* 2013 *Phys. Rev. Lett.* **110** 055003
[16] Staebler G M *et al* 2013 *Nucl. Fusion* **53** 113017
[17] Waltz R E, Dewar R L and Garbet X 1998 *Phys. Plasmas* **5** 1784
[18] Connor J W and Wilson H R 2000 *Plasma Phys. Control. Fusion* **42** R1
[19] Bishop C M 1986 *Nucl. Fusion* **26** 1063
[20] Rogers B N, Drake J F and Zeiler A 1998 *Phys. Rev. Lett.* **81** 4396
[21] Terry P W 2000 *Rev. Mod. Phys.* **72** 109
[22] Kim J *et al* 1994 *Plasma Phys. Control. Fusion* **36** A183
[23] Viezzer E *et al* 2014 *Nucl. Fusion* **54** 012003
[24] Fujisawa A 2009 *Nucl. Fusion* **49** 013001
[25] Hillesheim J C *et al* 2016 *Phys. Rev. Lett.* **116** 065002
[26] Sauter P *et al* 2012 *Nucl. Fusion* **52** 012001
[27] Shao L M *et al* 2016 *Plasma Phys. Control. Fusion* **58** 025004
[28] Hirshman S P and Sigmar D J 1981 *Nucl. Fusion* **21** 1079
[29] Callen J D, Cole A J and Hegna C C 2009 *Nucl. Fusion* **49** 085021
[30] Wu X Q *et al* 2015 *Nucl. Fusion* **55** 053029
[31] Diamond P H and Kim Y B 1991 *Phys. Fluids* B **3** 1626
[32] Morris R C, Haines M G and Hastie R J 1996 *Phys. Plasmas* **3** 4513
[33] McDevitt C J *et al* 2010 *Phys. Plasmas* **17** 112509
[34] Rozhansky V and Tendler M 1992 *Phys. Fluids* B **4** 1877
[35] Rozhansky V A *et al* 2001 *Nucl. Fusion* **41** 387
[36] Xu G S *et al* 2014 *Nucl. Fusion* **54** 103002
[37] Pitcher C S and Stangeby P C 1997 *Plasma Phys. Control. Fusion* **39** 779
[38] LaBombard B *et al* 2004 *Nucl. Fusion* **44** 1047
[39] Kim J *et al* 1994 *Phys. Rev. Lett.* **72** 2199
[40] Xu G S *et al* 2011 *Phys. Rev. Lett.* **107** 125001
[41] Muller S H *et al* 2014 *Phys. Plasmas* **21** 042301
[42] Cheng J *et al* 2013 *Phys. Rev. Lett.* **110** 265002
[43] Xu G S *et al* 2009 *Nucl. Fusion* **49** 092002
[44] Manz P *et al* 2012 *Phys. Plasmas* **19** 072311
[45] Tynan G R *et al* 2013 *Nucl. Fusion* **53** 073053
[46] Yan Z *et al* 2014 *Phys. Rev. Lett.* **112** 125002
[47] Cziegler I *et al* 2014 *Plasma Phys. Control. Fusion* **56** 075013
[48] Xu G S *et al* 2014 *Nucl. Fusion* **54** 013007
[49] Shao L M *et al* 2013 *Plasma Phys. Control. Fusion* **55** 105006
[50] Nielsen A H *et al* 2015 *Phys. Lett.* A **379** 3097
[51] Rasmussen J J *et al* 2016 *Plasma Phys. Control. Fusion* **58** 014031
[52] Xu X Q *et al* 2000 *Phys. Plasmas* **7** 1951
[53] Xia T Y, Xu X Q and Xi P W 2013 *Nucl. Fusion* **53** 073009
[54] Li B *et al* 2015 *Phys. Plasmas* **22** 112304
[55] Waltz R E *et al* 1995 *Phys. Plasmas* **2** 2408
[56] Waltz R E, Kerbel G D and Milovich J 1994 *Phys. Plasmas* **1** 2229
[57] Doyle E J *et al* 1991 *Phys. Fluids* B **3** 2300
[58] Xu G S *et al* 2016 *Phys. Rev. Lett.* **116** 095002
[59] Frieman E A and Chen L 1982 *Phys. Fluids* **25** 502
[60] Staebler G M and Groebner R J 2015 *Plasma Phys. Control. Fusion* **57** 014025
[61] Staebler G M and Groebner R J 2015 *Nucl. Fusion* **55** 073008